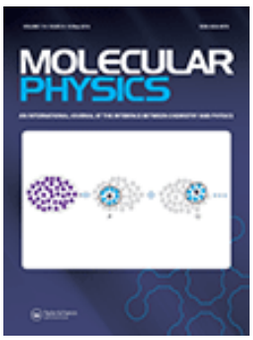

Taylor & Francis
Taylor & Francis Group

Molecular Physics

An International Journal at the Interface Between Chemistry and Physics

ISSN: 0026-8976 (Print) 1362-3028 (Online) Journal homepage: http://www.tandfonline.com/loi/tmph20

Propagation of nonstationary electronic and nuclear states: attosecond dynamics in LiF

Ksenia G. Komarova, F. Remacle & R. D. Levine

To cite this article: Ksenia G. Komarova, F. Remacle & R. D. Levine (2018): Propagation of nonstationary electronic and nuclear states: attosecond dynamics in LiF, Molecular Physics, DOI: 10.1080/00268976.2018.1451932

To link to this article: https://doi.org/10.1080/00268976.2018.1451932

MOLECULAR PHYSICS, 2018
https://doi.org/10.1080/00268976.2018.1451932

Taylor & Francis
Taylor & Francis Group

MICHAEL BAER FESTSCHRIFT

Propagation of nonstationary electronic and nuclear states: attosecond dynamics in LiF

Ksenia G. Komarova [a], F. Remacle [a,b] and R. D. Levine[a,c]

[a]The Fritz Haber Center for Molecular Dynamics and Institute of Chemistry, The Hebrew University of Jerusalem, Jerusalem, Israel; [b]Theoretical Physical Chemistry, UR MolSys B6c, Université de Liège, Liège, Belgium; [c]Department of Molecular and Medical Pharmacology, David Geffen School of Medicine and Department of Chemistry and Biochemistry, University of California, Los Angeles, CA, USA

ABSTRACT

Rapid optical excitation of a molecule produces a nonstationary state localised in the Franck–Condon region. To move out of that region, one needs to propagate both the electronic and the nuclear state. We formulate the motion on a grid of nuclear coordinate. The coupling to the electric field is fully included in the Hamiltonian used for propagation. We use perturbation theory to analyse the results of dynamics from one grid point to another. The nonadiabatic coupling terms arise from propagating the electronic states. We apply the formalism to the simple case of a diatomic molecule in an approximate but accurate scheme that allows performing computation on a limited number of grid points. As the coherent dynamics unfolds, we expand the grid in the direction of the wave packet motion with the quantum chemical calculations of the electronic structure performed 'on the fly'. The LiF molecule excited by a one-cycle IR pulse is used as a computational example. The 30-fs propagation through the crossing of the ionic and covalent states is overall adiabatic. The role of electron–nuclear coherences is emphasised.

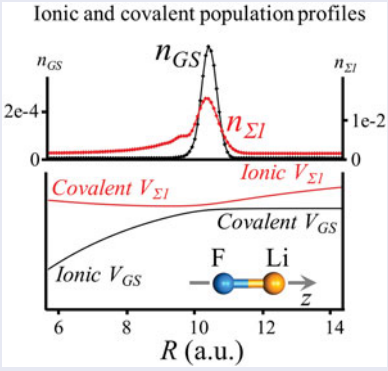

ARTICLE HISTORY
Received 9 February 2018
Accepted 2 March 2018

KEYWORDS
Post Born–Oppenheimer; nonadiabatic dynamics; discrete variable representation; finite difference approximation; avoided curve crossing

Introduction

A classical trajectory moves under a force generated as a gradient of a potential. In the Born–Oppenheimer approximation, this local potential is the electronic energy at a given configuration of the atoms. In an approach 'on the fly', the classical trajectory is propagated one step at a time. The electronic energy is computed for the new position, the trajectory is moved to the next point and so on. This is made possible because a computation that reliably gets the energy also can get the gradient of the potential [1]. Computing the electronic energy is typically the rate limiting step in the simulation of the dynamics. To make as few such energy computations as possible is a key advantage of computing 'on the fly' because the energy is only needed at the actual configurations accessed by the motion. In this paper, we deal with dynamics on several electronic states. It is then necessary to go beyond Born-Oppenheimer approximation [2,3] and to propagate the nuclei quantum mechanically. But we do seek to retain the advantage of the 'on the fly' computations because even for quantal dynamics, it is computing the electronic states at each nuclear configuration of interest that remains the bottleneck.

We consider a fast optical excitation. Initially, the excited system is localised in the Franck–Condon region

CONTACT Ksenia G. Komarova kgvladi@fh.huji.ac.il
Supplemental material for this article can be accessed at https://doi.org/10.1080/00268976.2018.1451932.

as determined by the ground state (GS). By propagation, we, therefore, mean the change in the atomic configuration of the system as it moves out of the Franck–Condon region. If the energy is not sufficient for dissociation, the system can return to the Franck–Condon region and move out again, etc.

As a numerical example, we analyse the performance of the 'on the fly' computation for the case of dynamics in LiF pumped with an attosecond linearly-polarised IR-pulse. The coupling to the electric field is fully included in the Hamiltonian used for the propagation. In this molecule, ground and first excited Σ electronic states provide an example of two states with avoided crossing at a long internuclear distance [4,5]. The change in the ionic character of the adiabatic states while going through the crossing is reflected by a high nonadiabatic coupling term τ_{12} , as was systematically examined within quantum chemical (QC) computations [6]. During our dynamical simulations, we stay in the adiabatic electronic basis with all nonadiabatic effects fully taken into account. Moving to the diabatic representation has clear benefits (see, for example, the discussion in [7]). But while computing 'on the fly', the adiabatic to diabatic transformation is not as accurate, since only a restricted number of points on the nuclear grid are available for the analysis of the electronic configuration.

Theoretical methodology

We consider first propagating the electronic states. In the Born–Oppenheimer approximation, this is clear. In every configuration of the atoms, the electronic states are eigenfunctions of the electronic Hamiltonian for that configuration. This is usually described as the very rapidly moving electrons instantaneously adjusting to the motion of the nuclei. Such an adiabatic approximation is technically described [8] as the neglect of the derivative with respect to the changes in position of the atoms of the transformation of the electronic states from one configuration to another. To prepare for the intended application, consider a nonrotating diatomic molecule so that the propagation is one dimensional. Then introduce a grid [9] along the bond distance where the grid points are a (short) distance a apart. We use the index i for the grid point located at the position x_i. $\boldsymbol{\psi}_k(x_i)$ is the kth electronic eigenstate at the grid point i. Assume that we have a complete set of electronic states at every grid point. Then the electronic wave function at the point i + 1 is related to that at the point i by the transformation $|\boldsymbol{\psi}_k(x_{i+1})\rangle = \sum_l |\boldsymbol{\psi}_l(x_i)\rangle\langle\boldsymbol{\psi}_l(x_i)|\boldsymbol{\psi}_k(x_{i+1})\rangle$. In the adiabatic approximation, the electronic state changes continuously so that the off-diagonal elements satisfy $\partial\langle\boldsymbol{\psi}_l(x_i)|\boldsymbol{\psi}_k(x_i+a)\rangle/\partial x \cong 0$.

Mathematically, one can represent the propagation of the electronic states using a Taylor expansion.

$$\begin{aligned}\left|\boldsymbol{\psi}_k(x_{i+1})\right\rangle &= \left|\boldsymbol{\psi}_k(x_i)\right\rangle + a\left|\partial\boldsymbol{\psi}_k(x)/\partial x\right\rangle|_{x=x_i} \\ &+ \left(a^2/2\right)\left|\partial^2\boldsymbol{\psi}_k(x)/\partial x^2\right\rangle|_{x=x_i} + \ldots\end{aligned} \tag{1}$$

Keeping terms to second-order is sufficient to evaluate the terms neglected to order a in the adiabatic approximation.

$$\begin{aligned}&\partial\left\langle\boldsymbol{\psi}_l(x+a)\right|\left|\boldsymbol{\psi}_k(x)\right\rangle/\partial x \cong a\partial\left\langle\partial\boldsymbol{\psi}_l(x)/\partial x\right|\left|\boldsymbol{\psi}_k(x)\right\rangle/\partial x \\ &= a\left\langle\partial^2\boldsymbol{\psi}_l(x)/\partial x^2\right|\left|\boldsymbol{\psi}_k(x)\right\rangle + a\left\langle\partial\boldsymbol{\psi}_l(x)/\partial x\right|\left|\partial\boldsymbol{\psi}_k(x)/\partial x\right\rangle\end{aligned} \tag{2}$$

Alternatively, one can evaluate the change in the electronic state using perturbation theory. When the step size a is small, the change in the Hamiltonian, the perturbation between two adjacent sites, is $\Delta H = H(x_{i+1}) - H(x_i) \cong a\partial H/\partial x$. The first-order correction to the wave function $|\boldsymbol{\psi}_k(x_i)\rangle$, assuming no degeneracy, is a linear combination of the other, $l \neq k$, electronic eigenfunctions $|\boldsymbol{\psi}_l(x_i)\rangle$, $H(x_i)|\boldsymbol{\psi}_l(x_i)\rangle = \mathbf{E}_l(x_i)|\boldsymbol{\psi}_l(x_i)\rangle$, at the same location,

$$\begin{aligned}\left|\boldsymbol{\psi}_k(x_{i+1})\right\rangle &= \left|\boldsymbol{\psi}_k(x_i)\right\rangle \\ &+ a\sum_{l\neq k}\left|\boldsymbol{\psi}_l(x_i)\right\rangle\frac{\left\langle\boldsymbol{\psi}_l(x_i)\right|\partial H_i/\partial x\left|\boldsymbol{\psi}_k(x_i)\right\rangle}{\mathbf{E}_k(x_i) - \mathbf{E}_l(x_i)}\end{aligned} \tag{3}$$

This is the same result as from the Taylor expansion because of the well-known identity

$$\left\langle\boldsymbol{\psi}_m(x_i)\right|\partial\boldsymbol{\psi}_k(x_i)/\partial x\right\rangle = \frac{\left\langle\boldsymbol{\psi}_m(x_i)\right|\partial H_i/\partial x\left|\boldsymbol{\psi}_k(x_i)\right\rangle}{\mathbf{E}_k(x_i) - \mathbf{E}_m(x_i)} \tag{4}$$

Baer [2] uses the notation

$$\tau_{mk} \equiv \hbar\left\langle\boldsymbol{\psi}_m(x_i)\right|\partial\boldsymbol{\psi}_k(x_i)/\partial x\right\rangle. \tag{5}$$

See also Smith [10]. Terms that are conventionally regarded as the Born–Oppenheimer correction to the nuclear dynamics, e.g. [11], are seen to arise from the nonadiabatic corrections to the propagation of the electronic state. This difference arises because we have another kind of perturbation. Born and Oppenheimer [11] use the kinetic energy of the nuclei as the perturbation. We describe the wave functions on a discrete grid. So, we use the change in the electronic Hamiltonian between two adjacent grid points, $a\partial H/\partial x$, as the perturbation. To lowest order, the change in energy due to the perturbation is the gradient of the potential scaled by a. Therefore, the spacing of the grid needs to take into

account the steepness of the potential in the region of interest.

Next we need to propagate the nuclear wave functions on the grid. Can we confine the propagation to near neighbours? The action of the nuclear kinetic energy operator is usually evaluated by transforming the wave function of the grid to the momentum space [12]. There the action of the kinetic energy operator is a local multiplication by $\hbar^2k^2/2m$. But the transformation to momentum space requires knowing the nuclear wave function throughout the grid. A possible alternative is to evaluate the derivatives in the momentum and the kinetic energy operators using a finite difference expression [9]. In the supplementary information, we briefly outline these expressions using only near neighbours (which is correct to order of a^2) and also the results using next near neighbours. The nuclear kinetic energy operator $\hat{T}$ has the matrix elements in the electronic basis when we use only near neighbours.

$$\begin{aligned}\langle \boldsymbol{\psi}_k(x_i)|\ \hat{T}\ |\ \boldsymbol{\psi}_l(x_j)\rangle &= -\boldsymbol{\delta}_{kl}\left(\hbar^2/2ma^2\right)\left(\boldsymbol{\delta}_{i,j-1}-2\boldsymbol{\delta}_{i,j}+\boldsymbol{\delta}_{i,j+1}\right)\\ &-\left(\hbar^2/2ma\right)\langle \boldsymbol{\psi}_k(x_i)|\ \partial\boldsymbol{\psi}_l(x_i)/\partial x\rangle\left(\boldsymbol{\delta}_{i,j+1}-\boldsymbol{\delta}_{i,j-1}\right)\\ &-\left(\hbar^2/2m\right)\langle \boldsymbol{\psi}_k(x_i)|\ \partial^2\boldsymbol{\psi}_l(x_i)/\partial x^2\rangle\boldsymbol{\delta}_{i,j}\end{aligned} \tag{6}$$

To write the complete wave function $\boldsymbol{\Psi}$, we define $C_{ni}(t)$ as the amplitude of the nuclear wave function in electronic state n at the grid point i at the time t.

$$\boldsymbol{\Psi} = \sum_n \sum_i C_{ni}(t)\boldsymbol{\psi}_n(x_i) \tag{7}$$

The time-dependent Schroedinger equation for the full wave function yields an equation of motion for the nuclear amplitudes:

$$\begin{aligned}i\hbar\frac{dC_{ni}}{dt} &= \left(\left(\hbar^2/ma^2\right)+V_{nn}(i)-E\,(t)\,\mu_{nn}\,(i)\right)C_{ni}\\ &-\left(\hbar^2/2ma^2\right)\left(C_{ni-1}+C_{ni+1}\right)\\ &-\sum_{k\neq n}(E(t)\mu_{nk}(i)C_{ki}-(\hbar/2ma)\tau_{nk}(i)(C_{ki-1}-C_{ki+1})\\ &+(1/2m)Y_{nk}(i)C_{ki})\end{aligned} \tag{8}$$

Here $E(t)$ is the pumping optical field, that for a one- or few-cycle pulse, acts only for a brief duration. $\mu_{nn}(i)$ is the dipole of the electronic state n at the grid point i while $\mu_{nm}(i)$ is the transition dipole from state n to m, at the grid point i. $Y_{nk}(i) = \hbar^2\langle\boldsymbol{\psi}_n(x_i)|\partial^2\boldsymbol{\psi}_k(x_i)/\partial x^2\rangle$, see Equation (6), are the nonadiabatic coupling terms of the second-order.

As Smith [10] and Baer [2] noted, the nonadiabatic terms can be added to the nuclear momentum operator $\hat{P}$ giving rise to a generalised momentum $\hat{\wp} = \hat{P} + p$, where $p = -i\tau$. The validity of the Born–Oppenheimer separation requires that τ is small as compared to the local momentum, $|i\hbar(C_{ki-1} - C_{ki+1})|/2a$, see Equation (8). This is consistent with our perturbation expansion, Equation (3).

The role of the nonadiabatic terms in driving the motion of the nuclei is seen also when we compute the force as the rate of change of the nuclear momentum.

$$\begin{aligned}(i\hbar)^{-1}\langle\boldsymbol{\Psi}|\,[\hat{P},\hat{H}]\,|\boldsymbol{\Psi}\rangle &= \sum_{i,k}|C_{ik}|^2(-\partial V_{ik}/\partial R)\\ &+(1/2ma)\sum_{i,k\neq l}(C^*_{ki}C_{li-1}-C^*_{ki}C_{li+1})(\partial\tau_{kl}(i)/\partial R)\end{aligned} \tag{9}$$

In the presence of the optical field, there are additional terms when the nuclei are driven by the field; see the supplemental material. The force on the nuclei is seen to be given as a classical-like average over the force of the motion on the different electronic states plus a term reflecting the nonadiabatic contribution. This second term depends on the interference between the amplitudes of the nuclear wave packets in different electronic states. The coupling coefficient, $1/2ma$, decreases at higher masses.

The equation of motion (8) completes our theoretical program. It expresses the propagation of the nuclear amplitude at grid point i in terms of the propagation to the two adjacent neighbouring points of the grid. The first (top) line in the equation of motion (8) is diagonal in the electronic index n. The first term in this secular part, $(\hbar^2/ma^2)$, is the local and electronically diagonal kinetic energy. It acts to change only the phase of the amplitude. The last two terms are the transfer of amplitude to the two adjacent grid sites while keeping the electronic state n. It is an adiabatic transfer. The second line in the equation of motion is the electronically nonadiabatic terms. The change of electronic state can be induced by the optical field if it is acting at the time t. Beyond this, the change is due to the terms that are the propagation of the electronic state.

Retaining five terms in a finite difference expression for the second derivative is equivalent to propagating the electronic state to order a^4. The corresponding equation of motion has more terms than (8) where each grid point is coupled only to its two immediate neighbours. But even for the more accurate five point kinetic energy, a grid point is coupled only to the two near neighbour points on either side.

The three or five point coupling is very localised and allows computing 'on the fly' in a manner that mimics the classical version. As in classical mechanics, one can initiate the quantal propagation from just a single grid

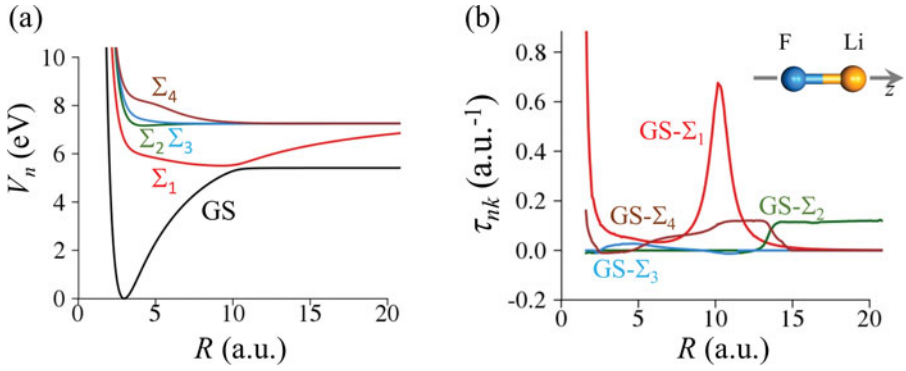

Figure 1. Adiabatic potentials (a) and nonadiabatic couplings of the first-order τ_{nk} (b) for a set of lowest Σ states as a function of internuclear distance in LiF, as calculated at the MRCI/SA5-CAS SCF level. The sign of τ_{nk} is determined by the orientation of the Li–F that is set along the z-axis as shown in (b).

point being initially occupied. But such an initial state is not physically realistic in either quantum or classical mechanics. In simulating a typical photochemical propagation, the initial conditions are often the stationary ground vibrational state of the ground electronic state. Then, one needs to switch the field on. So, we select the values of the nuclear amplitudes C_{ni} to vanish on all but the ground electronic state. On the GS, the amplitudes are either generated numerically or fitted to an analytical form of, say, a Morse vibrational state [13]. To generate the amplitudes numerically, one should take advantage of established experience and initiate the integration in the classically forbidden region on the left. Say, one disregards the conventional wisdom and starts the integration in the middle of the Franck–Condon region. The method will recover the GS wave function but only after a completion of more than one orbit so that destructive interference can filter out the undesirable components. This of course takes time. So, instead one can take advantage of multigrid methods [14] to filter out the high momentum components. However one proceeds, the light pulse should not be switched on before one has a reasonable approximation for the initial state.

There is a practical consideration in favour of extending a state localised on the grid by more than one grid point at a time. One can then perform in parallel the computations of electronic states for several adjacent grid points at a time. Since these computations are the bottleneck, a multipoint grid extension is advantageous in terms of the overall computing time.

Computational details

Quantum chemical computations

GS and four lowest excited states of Σ symmetry were chosen to represent the electronic wave packet of the time-dependent wave function. Higher excited states lie 10 eV further above the GS [15], which corresponds to more than six photons for the IR-excitation (1.5 eV per photon). At our laser intensity (as follows), these states will be much less populated compared to the lower-lying states (which have ∼ 6–8 eV excitation energy, see Figure 1(a)).

At equilibrium distance, ionic GS of LiF is described by configuration $\{1\sigma^2 2\sigma^2 3\sigma^2 4\sigma^2 1\pi^4\}$, where the σ orbitals are predominantly the 1s(F), 1s(Li), 2s(F) and $2p_z$(F) orbitals, respectively, while the π orbital is mostly $2p_{x,y}$(F). In all the low-lying excited states of interest, compared to the GS, electron density has moved from the F atom to the Li. At the geometry of the GS, the first Σ excited state is covalent. At a large distance (at about 10 a.u. for the computational level used here), there is an avoided crossing between the GS and the first excited Σ state [4,5]. The GS becomes essentially covalent while the first excited state is ionic. The change in the bonding character of these states while going through the crossing is reflected by the high nonadiabatic coupling term τ_{12}. As it was shown in [6], the position of the crossing is varying within 1–2 a.u. depending on the accuracy of the description of the dynamical correlation by the chosen QC method of computation. We use here the methodology of Reference [6] that was shown to give accurate results for the description of the ground and first excited state. The matrix elements of the electronic Hamiltonian are calculated using a state-averaged full-valence CAS SCF [16,17] followed by internally contracted MRCI [18,19] as implemented in the MOLPRO package [17]. The correlation-consistent cc-pVQZ and aug-cc-pVQZ Dunning basis sets [20,21] were used for Li and F, respectively. The core 1s(F), 2s(F) and 1s(Li) molecular orbitals were kept inactive, as it was shown that they have minor effect in the description of the avoided crossing [6]. The active space consists of 6 electrons distributed among

7 orbitals, which yields 142 CSF for the reference CAS SCF wave function. The state-averaging procedure was carried out for all the five states with equal weights. If only two states, the excited Σ_1 and the GS are included in the state-averaging, the avoided crossing lies around 13.2 a.u., which is in good agreement with previous results [6,15]. When the averaging is active for all five states, the position of the crossing is occurring at the shorter distances (∼10 a.u., see Figure 1(a)) because of a less accurate description of the GS. In what follows, we refer to it as MRCI/SA5-CAS SCF computation.

The first-order nonadiabatic coupling term takes large values in the region of the covalent-ionic avoided crossing (Figure 1(b)). These values as well as the potential energies are similar to those computed for only two state averaging [5]. Therefore, except for the shift of the avoided crossing, there are only minor effects on the dynamics that followed the excitation in the five state CAS averaged procedure.

On the fly propagation on the grid

The amplitudes of each electronic basis function defined on the grid of Li–F internuclear distances are propagated in time using Runge–Kutta fourth-order scheme. In all calculations, we define the molecular orientation such that the origin of the molecular frame is at the nuclear centre of mass and the Li atom is in the positive direction of the z-axis. We start initially from a few grid points – 26 points spanning a range of internuclear distances from 2 to 4 a.u. – a range large enough for an accurate description of the GS wave function and the field-induced population of the excited states within the Franck–Condon region. As the wave packets on the excited states begin to move, the population close to the edge of the grid is growing. We expand the grid only if the population at the edge becomes larger than some predefined threshold. Due to the localised form of the momentum and kinetic energy, this affects only coefficients at the edge of the grid. The error is on the order of the values of the amplitudes multiplied by the coupling constants ($\hbar\tau/2ma$ or $\hbar^2/2ma^2$ for momentum and kinetic terms, respectively).

Each time we extend the grid – we compute the matrix elements only at the additional points and restart the dynamics from previous coefficients on the new, larger grid. For each state, the threshold is defined by comparison of the population at the edge – to the maximum of the population of this state in the region of 1 a.u. from the edge. This distance seems reasonable for the localised wave packets, which are created by pumping with an ultrashort pulse. However, during the dynamics on each excited state, the width is changing according to the curvature of the potential [22]. In the present case, the threshold of 5% for the grid extension provides a good accuracy of the overall dynamics. As a benchmark (we refer to it as 'full grid' computation), we use results of the propagation on the initially large grid of 356 points spanning the range (1.6, 30) a.u. with a grid spacing of $a = 0.08$ a.u.

Details of the propagation procedure

Interaction with pulse was explicitly taken into account in the Hamiltonian, using the time profile of the electric field:

$$\begin{aligned}\mathbf{E}_p(t) &= (-1/c)\,\partial A_p(t)/\partial t = \\ &= \mathbf{E}_p \exp\left(-(t-t_p)^2/2{\sigma_p}^2\right) \\ &\quad\times\left(\cos(\omega_p t) - \frac{(t-t_p)}{\omega_p\sigma_p^2}\sin(\omega_p t)\right) \quad (10)\end{aligned}$$

$$A_p = -\frac{\mathbf{E}_p c}{\omega_p}\exp\left(-(t-t_p)^2/2{\sigma_p}^2\right)\sin(\omega_p t) \quad (11)$$

where $\mathbf{E}_p(t)$ is electric field, which corresponds to the vector potential A_p. The direction of the pulse is chosen to be along the F–Li vector, $\mathbf{E}_p = |\mathbf{E}_z^p|e_z$, with an amplitude $|\mathbf{E}_z^p| = 0.08$ a.u. that ensures hardly any population in the higher electronically excited states. The frequency of the pulse ω_p was set to be 800 nm, with $\sigma_p = 20$ a.u. of time. This narrow width means that it is an essentially one-cycle pulse.

The representation of the GS wave function on the grid was defined using an analytical expression of the anharmonic wave function, which corresponds to the fit of the Morse potential to the calculated GS potential ($D_e = 5.5$ eV, $\alpha = 0.6$ a.u., $R_e = 3.00$ a.u.). The time step for the propagation was set to 0.01 a.u. of time, except the region of avoided crossing, where 10 times lower time-step was needed to conserve the norm of the time-dependent wave function. The electron–nuclear dynamics is described in terms of time-dependent population $n_k(t)$ of each electronic state, defined by

$$n_k(t) = \sum_i n_{ki}(t) = \sum_i |C_{ni}(t)|^2 \quad (12)$$

The time-dependent dipole moment has contribution both from diagonal components of the density matrix (due to nonzero permanent dipoles of the electronic states) and off-diagonal components weighted by the transition dipole between the states:

$$\begin{aligned}\mu_{tot}(t) &= \sum_{n,i} n_{ki}(t)\,\mu_{nn}(i) \\ &\quad + \sum_{n,k,i}\left[C_{ni}^*(t)\,C_{ki}(t) + C_{ki}^*(t)\,C_{ni}(t)\right]\mu_{nk}(i) \quad (13)\end{aligned}$$

Results and discussion

Low-lying Σ excited states in LiF can be divided in two groups with main excitations from the $2p_z$ (Σ_1, Σ_4 states, Figure 2(a)) and $2p_{x,y}$ (Σ_2, Σ_3 states, Figure 2(b)) atomic orbitals localised on the F atom to the orbitals of the Li atom of the respective symmetry. At the equilibrium geometry of the GS, each pair has similar determinants in the CAS SCF wave function with opposite sign for the low-lying states (Σ_1, Σ_2) and the same sign for the states of higher energy (Σ_4, Σ_3). For the first group, this composition results in the alternation of the permanent dipole: −3.6 Debye in Σ_1 and 4 Debye in Σ_4 state (Figure 2(a)). Also the transition dipoles for GS–Σ_1 and GS–Σ_4 excitation have opposite signs.

In the second group, Σ_2 state with opposite signs of the $\pi_x \rightarrow \pi_x^*$ and $\pi_y \rightarrow \pi_y^*$ determinants becomes a fully dark state for excitations from the GS (Figure 2(c)) while Σ_3 state being the sum of them has the largest transition dipole from GS. This enables us to choose the parameters of the one-cycle pulse in such a way that specific excited states will be preferentially populated. Taking a linearly-polarised pulse in the positive z-direction yields significant excitation of Σ_1 excited state while a setting negative polarisation direction gives rise to the population of Σ_4 state. In both cases, Σ_3 state is also significantly populated due to its large GS–Σ_3 transition dipole and the fact that there are two secondary maxima in the short IR pulse (see Figure 3). Here, we report the dynamics upon pumping in positive direction, so as to discuss the effects of the nonadiabatic coupling between Σ_1 and GS.

Overall, Figure 3 shows that the electronic states are able to respond almost but not quite adiabatically to the IR field, meaning that net excited state populations at the end of the interaction with the pulse is smaller than population during the pulse. See in particular the population of the most highly accessed Σ_3 state. The population of this and also the other states, do respond on a time scale that is somewhat faster than the period of the 1.5-eV IR field. These rapid changes in the direction of the transfer (when the field $E(t)$has similar values) come from the change in sign of the imaginary part of the interelectronic coherences: $-E(t)\mu_{nk}(i)\mathrm{Im}(C_{ni}^* C_{ki})$ (see Equation (6) of the supplemental material). Because of the intermediate behaviour, neither fully adiabatic nor sudden we do treat the coupling to the field exactly by including it in the Hamiltonian.

Results of the 'on the fly' and full grid simulations of the population dynamics followed upon excitation with a pulse are shown in Figure 3, revealing the reliably high accuracy of the 'on the fly' computations (for the quantitative errors, see Figure S1 of the supplemental material). Due to dissociative nature of the excited state potentials, shortly after excitation, the wave packets move out of the Franck–Condon region (see movie M1 of the supplemental material), so extension of the initial grid is needed after 16 fs of the dynamics. The initial widths of the wave packets in the excited states resemble the narrow width of the GS wave function (around 1 a.u. in LiF). For the mostly populated Σ_1 and Σ_3 excited states, it stays within ∼1–2 a.u. during 220 fs of the dynamics. After that, Σ_1 wave packet reaches the outer turning point of the potential and significantly widens on the way back to the Franck–Condon region. Due to delocalisation of the wave packet, one may want to lower down the threshold during the restart of the propagation at longer times. Within the first ∼100 fs, current settings for the threshold and extension length provide the restart of the 'on the fly' propagation, each ∼10 fs of the dynamics (Figure 4). In terms of the computational time, QC calculation for each grid point takes 10–20 min using one CPU while propagation of the wave function to the next extension takes less than a minute. As matrix elements of the electronic Hamiltonian at different grid points are independent, it is possible to run the required QC calculations simultaneously on several CPUs.

Once the field is over, the population of the states only changes due to nonadiabatic couplings. As shown in Figure 1(b), this coupling is primarily between the GS and Σ_1 and it is localised in the region of their avoided crossing. So, we limit considerations to the case when the field is over, and we have significant nonadiabatic coupling only between the two electronic states $|1\rangle$ and $|2\rangle$. From Equation (8), the amplitudes of the nuclear wave packet on state $|1\rangle$ is

$$\begin{aligned} i\hbar\frac{dC_{1i}}{dt} = &\left(\left(\hbar^2/ma^2\right) + V_{11}(i)\right)C_{1i} \\ &- \left(\hbar^2/2ma^2\right)\left(C_{1i-1} + C_{1i+1}\right) \\ &+ (\hbar/2ma)\tau_{12}(i)(C_{2i-1} \\ &- C_{2i+1}) - (1/2m)Y_{12}(i)C_{2i} \end{aligned} \tag{14}$$

Using also the complex conjugate of the wave function gives an equation of motion for the population n_{1i} of the state $|1\rangle$:

$$\begin{aligned} \frac{dn_{1i}}{dt} = &-\left(\hbar/ma^2\right)\left[\mathrm{Im}\left(C_{1i}^* C_{1i-1}\right) + \mathrm{Im}\left(C_{1i}^* C_{1i+1}\right)\right] \\ &+ \left(1/ma\right)\tau_{12}(i)\left[\mathrm{Im}\left(C_{1i}^* C_{2i-1}\right) - \mathrm{Im}\left(C_{1i}^* C_{2i+1}\right)\right] \\ &- \left(1/\hbar m\right)Y_{12}(i)\mathrm{Im}\left(C_{1i}^* C_{2i}\right) \end{aligned} \tag{15}$$

The change in the local population consists of the propagation along the grid but retaining the same adiabatic electronic state, first line, and due to nonadiabatic

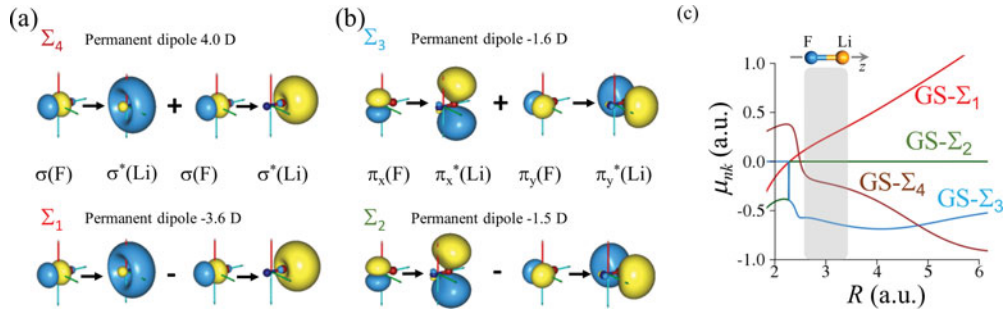

Figure 2. (a, b) Excitations between natural molecular orbitals of a_1(a) and b_1, b_2 (b) symmetry, which mainly contribute to the 4 lowest Σ excited states in LiF at the equilibrium geometry of the ground state (GS). Permanent dipoles are given for each state, the ground state permanent dipole is 6.4 D. (c) Transition dipole moments from the ground state as a function of internuclear distance. The area shaded in grey shows the Franck–Condon region.

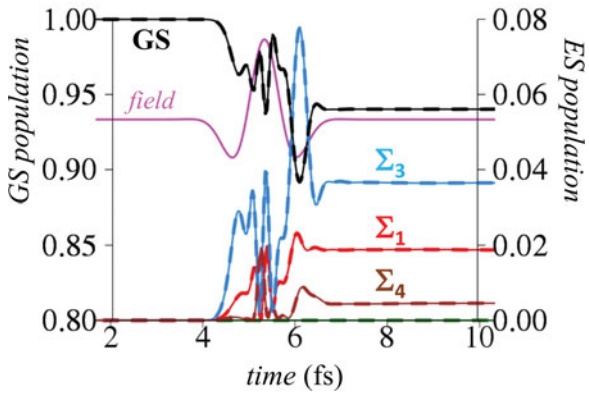

Figure 3. Nonequilibrium dynamics in LiF upon excitation with a one-cycle IR pulse (magenta line). Shown are results of the population dynamics computed for a grid spanning the entire range of *R* distance (1.6, 30 a.u.) (solid lines) and 'on the fly' (dashed lines). The figure illustrates the change in population in the Franck–Condon region and the short time exit from it. At longer times, the populations are essentially unchanged (Figure S1a of the supplemental material).

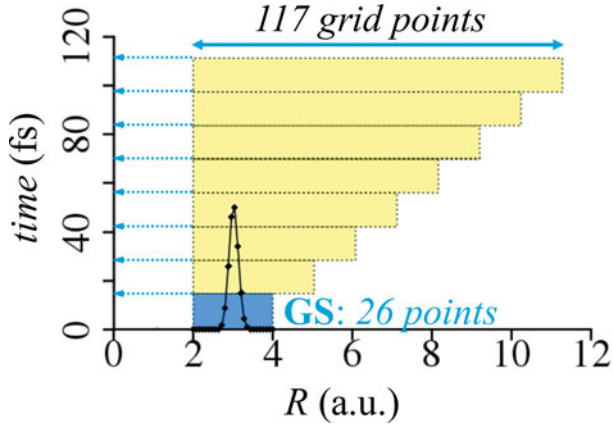

Figure 4. Regions of the internuclear distances taken into account at different time ranges of the dynamics during the 'on the fly' computation. The initial ground state (GS) wave packet was described using 26 points in a grid. After 120 fs of the dynamics, the size of the grid was extended to 117 grid points. The rather steep repulsion of the excited states is reflected in that the grid is only needed to be extended towards the way out.

transitions to the second state. Note the role of the coherence between adjacent points on the grid in the two lines.

Actual results for the local populations are shown in Figure 5. The figure is selected to emphasise the region where the nonadiabatic effects are strong. It shows the profiles of the wave packets on the GS and Σ_1 during the transversal of the avoided crossing superimposed on the two adiabatic potentials. These are for a full computation retaining the three lower lying excited electronic states. See the movie M2 in the supplemental material for the full view. Before the system reaches the avoided crossing, there is hardly any population on the GS at such large distances. Once the front end of the wave packet on Σ_1 reaches the range of the nonadiabatic coupling, it transfers amplitude to the GS. While the wave packet on Σ_1 moves forward, but remains in the region of a significant nonadiabatic coupling, the amplitude on the GS remains significant, Figure 5 panel (b). As the wave packet on Σ_1 moves out of the coupling region, panel (c), it recovers the amplitude it previously transferred to the GS. About 30 fs after the beginning of a population build-up on the GS in the avoided crossing region, it is empty again. At the same time, the wave packet on the Σ_1 states has recovered, and the population returns to its previous value. In summary, the transit through the avoided crossing region ends up adiabatic. The amplitudes before the entry are very similar in magnitude to the amplitude after the exit.

The duration of the transit through the avoided crossing region, τ, about 30 fs for the wave packet created by the one cycle pulse, is significantly longer than the time, τ_{el}, about 5 fs, required for transfer of amplitude between the two electronic states. The adiabaticity or lack thereof in a motion through the avoided crossing region

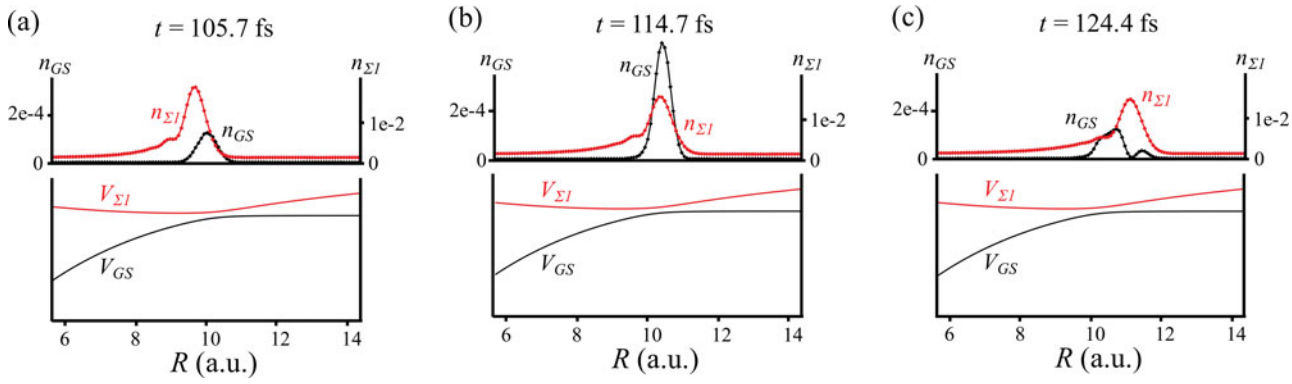

Figure 5. Population profiles as a function of internuclear distance R at different times (n_{GS}, $n_{\Sigma 1}$, top panel) and adiabatic potentials (lower panel) for the ground state (GS) and Σ_1 excited state of LiF in the region of the avoided crossing (around 10 a.u.). Shown are snapshots of the dynamics for the time of the initial population transfer to the ground state (a), its maximal value (b) and the time of the back-transfer of the population to the excited state (c).

was early on characterised quantitatively in the Landau–Zener model [23]. The probability P for an adiabatic passage was estimated as $P = \exp(-\pi^2\xi)$ where ξ is the adiabaticity parameter. A realistic estimate is $\xi = \tau/\tau_{el}$ of about 5 for the case of LiF as shown in the movie M2 and in three panels in Figure 5. The transit is therefore expected to be adiabatic and it is. This is such an adiabatic crossing that it is adiabatic at all realistic transit velocities. It is also seen in computations [5] of the collisional ionisation cross section in Li+F collision. The cross section is practically negligible. This is unlike, for example, a Li+I collision where the electron affinity of the iodine atom is much lower.

Summing over all grid points will give the overall change in population of the GS:

$$\frac{dn_1}{dt} = \frac{1}{m}\sum_i \{(\tau_{12}(i)/a)\left[\mathrm{Im}\left(C_{1i}^* C_{2i-1}\right) - \mathrm{Im}\left(C_{1i}^* C_{2i+1}\right)\right] - (Y_{12}(i)/\hbar)\mathrm{Im}\left(C_{1i}^* C_{2i}\right)\} \quad (16)$$

This is practically negligible in the case of LiF because the nonadiabatic terms first contribute with a positive sign – population of Σ_1 at the $(i+1)$ grid point is larger than at the point $(i-1)$, see Figure 5(a)). Later it comes with an opposite sign (Figure 5(c)) giving no significant net contribution to the sum.

At longer times, the wave packet on the bound but shallow Σ_1 potential broadens and is reflected from the outer turning point. At around 280 fs, its front edge reaches the avoided crossing region and begins to transfer population to the GS. The width of the upper wave packet is now larger and so the transit time is longer. The overall behaviour is now not quite as adiabatic as in the first passage because the GS potential is unbound and some population goes out to dissociation.

Conclusions

Quantum mechanical 'on the fly' computations of the dynamics of the motion on coupled electronic states is shown possible for a system whose configuration is described on a grid. Particular attention is given as to why it makes sense to propagate more than one grid step at a time. A minimal requirement for computing 'on the fly' is a sensible approximation of the momentum and the kinetic energy provided by coupling every point on the grid to its immediate near neighbours. This is sufficient to include the strong nonadiabatic coupling terms, which arise from the leading order extrapolation of the electronic states at a given location. It also includes coherence between the amplitude on a point and on the two neighbours. There are two such coherences. If the two points are on the same electronic state, this coherence describes the adiabatic propagation of the wave packet on the given state. But if the two points belong to two different electronic states, then the coherence describes the effect of the nonadiabatic coupling between them. In particular, the locally strong nonadiabatic coupling weighted by the coherence modifies the force acting on the nuclei so that it is not just the averaged sum of the forces in the different electronic states. A realistic and accurate 'on the fly' approximation includes also the next neighbouring points on the grid. This is sufficient to account even for strong nonadiabatic coupling. One-cycle IR laser pulse pumping LiF is an example showing no net population transfer, meaning an overall adiabatic behaviour. Yet, the local dynamics exhibit back and forth transfer between electronic states in the vicinity of an avoided crossing of the ionic and covalent states. The time-dependent local propagation shows that in LiF the rapid response of the electronic states is faster than the transit time through the avoided crossing region. Thereby, there is an

overall adiabatic behaviour despite quite active localised transitions.

Acknowledgment

We thank U.S. Department of Energy (DOE), Office of Science, Basic Energy Sciences (BES). FR thanks the FRS-FNRS for its support.

Disclosure statement

No potential conflict of interest was reported by the authors.

Funding

U.S. Department of Energy (DOE), Office of Science, Basic Energy Sciences (BES) [award number DE-SC0012628] and Fonds de la Recherche Fondamentale Collective [grant number T.0132.16], [grant number J.0012.18].

ORCID

Ksenia G. Komarova http://orcid.org/0000-0001-6603-1377
F. Remacle http://orcid.org/0000-0001-7434-5245

References

[1] X. Li, J.C. Tully, H.B. Schlegel, and M.J. Frisch, J. Chem. Phys. **123**(8), 084106 (2005). doi:10.1063/1.2008258.
[2] M. Baer, *Beyond Born-Oppenheimer: Electronic Nonadiabatic Coupling Terms and Conical Intersections*. (Wiley, Hoboken, NJ, 2006), pp. 39–44.
[3] R. Baer, J. Chem. Phys. **117**(16), 7405 (2002). doi:10.1063/1.1515768.
[4] R.S. Berry, J. Chem. Phys. **27**, 1288 (1957). doi:10.1063/1.1743993.
[5] M.B. Faist and R.D. Levine, J. Chem. Phys. **64**(7), 2953 (1976). doi:10.1063/1.432555.
[6] A.J.C. Varandas, J. Chem. Phys. **131**(12), 124128 (2009). doi:10.1063/1.3237028.
[7] H. Nakamura and D.G. Truhlar, J. Chem. Phys. **117**(12), 5576 (2002). doi:10.1063/1.1500734.
[8] R.D. Levine, *Quantum Mechanics of Molecular Rate Processes*. (Reprinted - Dover, Mineola, NY, 1999) (Oxford University Press, London, 1969).
[9] D.J. Tannor, *Introduction to Quantum Mechanics. A Time-Dependent Perspective* (University Science Books, Sausalito, CA, 2007).
[10] F.T. Smith, Phys. Rev. **179**(1), 111 (1969). doi:10.1103/PhysRev.179.111.
[11] M. Born and K. Huang, *Dynamical Theory of Crystal Lattices* (Clarendon Press, Oxford, 1954).
[12] R. Kosloff, J. Phys. Chem. **92**(8), 2087 (1988). doi:10.1021/j100319a003.
[13] P.M. Morse, Phys. Rev. **34**(1), 57 (1929). doi:10.1103/PhysRev.34.57.
[14] A. Brandt, Math. Comp. **31**(138), 333 (1977). doi:10.1090/S0025-5718-1977-0431719-X.
[15] K. Hanasaki and K. Takatsuka, Phys. Rev. A **88**(5), 053426 (2013). doi:10.1103/PhysRevA.88.053426.
[16] H.J. Werner and P.J. Knowles, J. Chem. Phys. **82**(11), 5053 (1985). doi:10.1063/1.448627.
[17] P.J. Knowles and H.-J. Werner, Chem. Phys. Lett. **115**(3), 259 (1985). doi:10.1016/0009-2614(85)80025-7.
[18] P.J. Knowles and H.-J. Werner, Chem. Phys. Lett. **145**(6), 514 (1988). doi:10.1016/0009-2614(88)87412-8.
[19] H.J. Werner, B. Follmeg, and M.H. Alexander, J. Chem. Phys. **89**(5), 3139 (1988). doi:10.1063/1.454971.
[20] T.H. Dunning, Jr., J. Chem. Phys. **90**(2), 1007 (1989). doi:10.1063/1.456153.
[21] R.A. Kendall, T.H. Dunning, Jr., and R.J. Harrison, J. Chem. Phys. **96**(9), 6796 (1992). doi:10.1063/1.462569.
[22] E.J. Heller, J. Chem. Phys. **62**(4), 1544 (1975). doi:10.1063/1.430620.
[23] R.D. Levine, *Molecular Reaction Dynamics* (Cambridge University Press, Cambridge, 2005).